Tuning the Optical Properties of Already Crystalized Hybrid Perovskite

Stav Rahmany, Monika Rai, Vitaly Gutkin, Małgorzata Wierzbowska, and Lioz Etgar*

The optical properties of halide perovskite are already tuned in the initial solution by choosing the preferred precursors. However, it is not obvious that the optical properties change following perovskite crystallization; moreover, the mechanism in this case is not clear. Herein, it is shown that the optical properties are not necessarily "fixed" following perovskite crystallization. The phenomenon using the halide exchange process in the solid phase of an already crystalized perovskite is demonstrated. The effects of formamidinium iodide (FAI) and formamidinium bromide (FABr) are investigated post-treatment on the physical, optical, and PV properties of $Cs_{0.2}FA_{0.8}Pb(I_{0.75}Br_{0.25})_3$ perovskite. Various FAI/FABr ratios in the post-treatment solutions show that a halide exchange occurs in the solid-state phase following the crystallization of the perovskite film. Energy-dispersive spectroscopy line scan made on focused ion beam samples show that the bromide is present deep inside the film post-treatment, which supports the fact that the reaction is not occurring only on the surface. Charge extraction and voltage decay measurements of the complete solar cells support the structural changes due to the halide exchange. This work enhances the knowledge of halide exchange in already crystalized perovskite.

1. Introduction

The need for green and environmentally friendly energy has paved the way for metal halide perovskite to be an excellent candidate to be used as a light harvester in solar cells. The metal halide perovskite displays attractive properties such as high absorption coefficient,[1,2] long diffusion lengths for charge carriers,[1,3,4] and a tunable band gap (E_g),[5–7] along with a variety of simple and easy deposition methods.[8–11] In the last several years, perovskite-based solar cells (PSCs) have shown a remarkable increase in terms of power conversion efficiency (PCE), exceeding 24%.[12]

Metal halide perovskite has an ABX_3 structure, where A is a monovalent cation ($MA^+ = $ methylammonium; $FA^+ = $ formamidinium, Cs^+, or Rb^+)[13,14] and B is a divalent rare metal (Pb^{2+} or Sn^{2+}) with a coordination number of 6 that forms a

BX_6 octahedron,[15,16] where X is a halide (I^-, Br^-, or Cl^-).[17] The composition of perovskite used today in state-of-the-art solar cells is based on double or triple cations (A site) with a mixture of halide, usually iodide and bromide.[13,18–20] The multi-cations in the perovskite are energetically favorable compared with a single-cation perovskite, as a result of reduced free energy due to an increase in the entropy of the system.[18] Moreover, multi-cation perovskites display high heat durability along with long-term stability and high PCE values.[21,22] The A site cations mainly stabilize the perovskite structure, whereas the halides dictate the optical properties of the perovskite, since their hybridization with the B cation orbitals determines the E_g value of the material.[23–25]

Further efforts are being made to improve the quality and electronic properties of the mixed cation/mixed halide perovskite to gain long-term stability and push the PCE toward the theoretical limit. One interesting approach to improve the quality of the perovskite film is by postdeposition interfacial engineering treatment. Nazeeruddin and co-workers demonstrated an improvement in the photovoltaic (PV) performance by treating the perovskite surface with formamidinium bromide (FABr), which converts unreacted PbI_2 to hybrid perovskite by forming a passivation layer that boosts the V_{oc} value.[26] A reduction in the hysteresis was reported by Yoo and Park,[27] using postdeposition treatment of phenyl-alkylammonium iodide. Wang demonstrated that formamidinium iodide (FAI) treatment can repair defects in halide vacancies and can improve the PCE in $MAPb(I_{0.95}Br_{0.05})_3$.[28] Rai et al. used a hot FAI dipping solution to enhance perovskite crystallinity and improve the surface coverage for semi-transparent solar cells.[29] As previously demonstrated by Grätzel et al., rapid halide exchange in the $MAPbX_3$ solid phase is possible while well preserving the morphology of the perovskite.[30] In this work, the

S. Rahmany, Dr. V. Gutkin, Prof. L. Etgar
Institute of Chemistry
The Center for Nanoscience and Nanotechnology
Casali Center for Applied Chemistry
The Hebrew University of Jerusalem
Jerusalem 91904, Israel
E-mail: lioz.etgar@mail.huji.ac.il

Dr. M. Rai
School of Material Science and Engineering
Nanyang Technological University
50 Nanyang Avenue, Singapore 639798, Singapore

Dr. M. Wierzbowska
Institute of High Pressure Physics
Polish Academy of Sciences
Sokołowska 29/37, 01-142 Warsaw, Poland

The ORCID identification number(s) for the author(s) of this article can be found under https://doi.org/10.1002/solr.201900128.

effect of postdeposition treatments on perovskite films composed of $Cs_{0.2}FA_{0.8}Pb(I_{0.75}Br_{0.25})_3$ was studied. The rationale of studying the $Cs_{0.2}FA_{0.8}Pb(I_{0.75}Br_{0.25})_3$ perovskite and not the pure α-$FAPbX_3$ is due to two main reasons: 1) the low stability of $FAPbX_3$ and 2) the presence of Cs^+ in the perovskite structure, which already displayed high PCEs.[18] The annealed perovskite films were dipped in a solution having different FAI/FABr ratios, to study the halide exchange in the solid phase of the perovskite. Interestingly, it was observed that the halide exchange occurs on the solid-state phase following the crystallization of the perovskite film. This is confirmed by the calculated formation energies, for the iodide substitution with Br, which are negative. The effect of FAI/FABr ratios on the optical properties, crystal structure, PV parameters, and stability was studied. High FABr ratios tend to reduce the quality of the perovskite film and agree with the picture of broken chemical bonds obtained from the theoretical structural optimization. This consequently affects the PV parameters of the solar cells.

2. Results and Discussion

In this work, we studied the halide exchange in a crystalized perovskite film. The first step includes depositing the perovskite on mesoporous TiO_2 by spin coating. The composition of the perovskite film was $Cs_{0.2}FA_{0.8}Pb(I_{0.75}Br_{0.25})_3$.

Following the completion of the perovskite crystallization (including its annealing), the film was dipped in a hot solution of isopropanol (IPA) that contains different ratios of FAI/FABr. The solar cell is completed by annealing and deposition of the hole transport material (HTM) and a gold contact. The whole process is shown in **Figure 1**. In this study, five different ratios of FAI/FABr were investigated including pure FAI and pure FABr. (Standard indicates without post-treatment.)

Replacing iodide with bromide will affect the optical properties of the perovskite, since the hybridization of the Pb^{2+} 6s orbitals with the Br^- 4p orbitals is low in energy compared with the hybridization with the I^- 5p orbitals, which results in a larger energy bandgap.[31,32] Powder X-ray diffraction (XRD) was performed to better understand the crystallographic changes in the already

crystalized perovskite film due to the postdeposition treatment (**Figure 2B**). The $FAPbBr_3$ perovskite has a cubic structure, whereas $FAPbI_3$ perovskite has a tetragonal crystal structure.[5,33] The peak at ≈14° is related to the <110> crystallographic plane of the perovskite, since when the FABr ratio in the dipping solution increases, the peak intensity is reduced and shifts toward 15° for the 25/75 (FAI/FABr) film. Moreover, the film that was treated with pure FABr solution displayed a split into two peaks around 15°, when the additional peak is related to the <110> plane of cubic $FAPbBr_3$.

A similar trend can be observed at ≈28°, which is related to the <002> crystallographic plane; in the case of the 25/75 (FAI/FABr) ratio, this peak shifts toward 29°. In the FABr-treated film there is a splitting into two peaks, which is related to the tetragonal $FAPbI_3$ (t-002) and cubic $FAPbBr_3$. Moreover, a shift toward higher angles for 25/75 and FABr post-treated films can be seen for the <001>, <111>, and <012> crystallographic planes, which are located at ≈20°, ≈24.5°, and ≈32°, respectively. The splitting of the XRD peaks in the case of high FABr ratios (pure FABr and 25/75) indicates that exchanging a large amount of iodide by bromide in the solid phase results in reduced crystallinity and partial distortion of the lattice, which can enhance the formation of defects in the mixed cation mixed halide perovskite. The peak intensity and full width at half maximum (FWHM) for 13–15° and for 28–30° as a function of the FAI/FABr ratios are plotted in Figures 2c,d, respectively. The trend is the same for both angle ranges, where there is more FABr in the dipping solution, and the peak intensity decreased and the FWHM increased. Both the widening and the decreasing intensities of the XRD peaks are shown in Figure S4A and S4B, Supporting Information. Therefore, it can be concluded that lower crystallinity and a partial distortion of the perovskite lattice appear in the case of post-treatment with an excess of FABr. The distortion of the crystal derives from the difference in the halide atomic radii. As previously shown,[18] when the mixed cation mixed halide perovskite lattice is formed, the different components are homogenously spread in the crystal; the X–Pb–X angle is slightly distorted due to the size difference between the two anions. Hence, the unit cell volume and the crystallographic plane distances are assumed to be fixed and organized along the lattice.
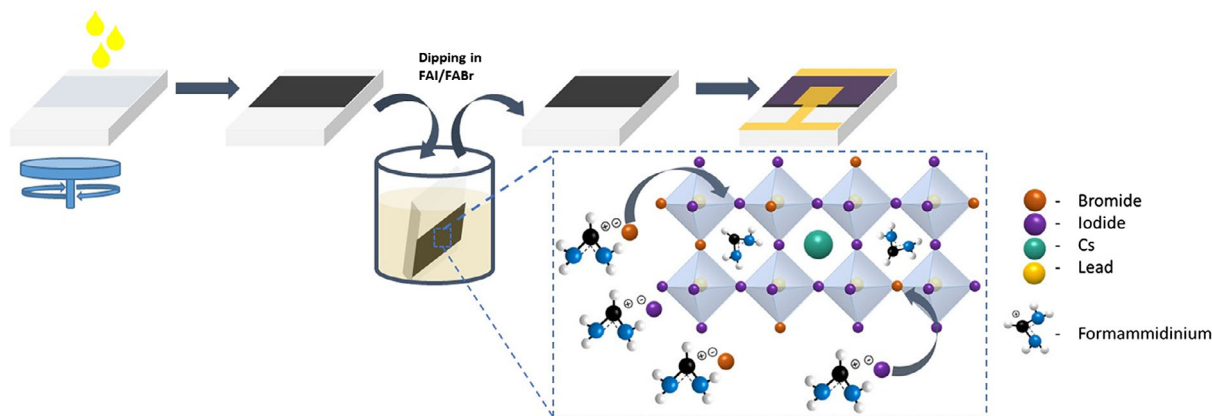

Figure 1. Schematic illustration of the mixed cation mixed halide perovskite deposition and postdeposition treatment. The dashed frame illustrates the halide exchange in the perovskite solid phase as a result of the post-deposition treatment.
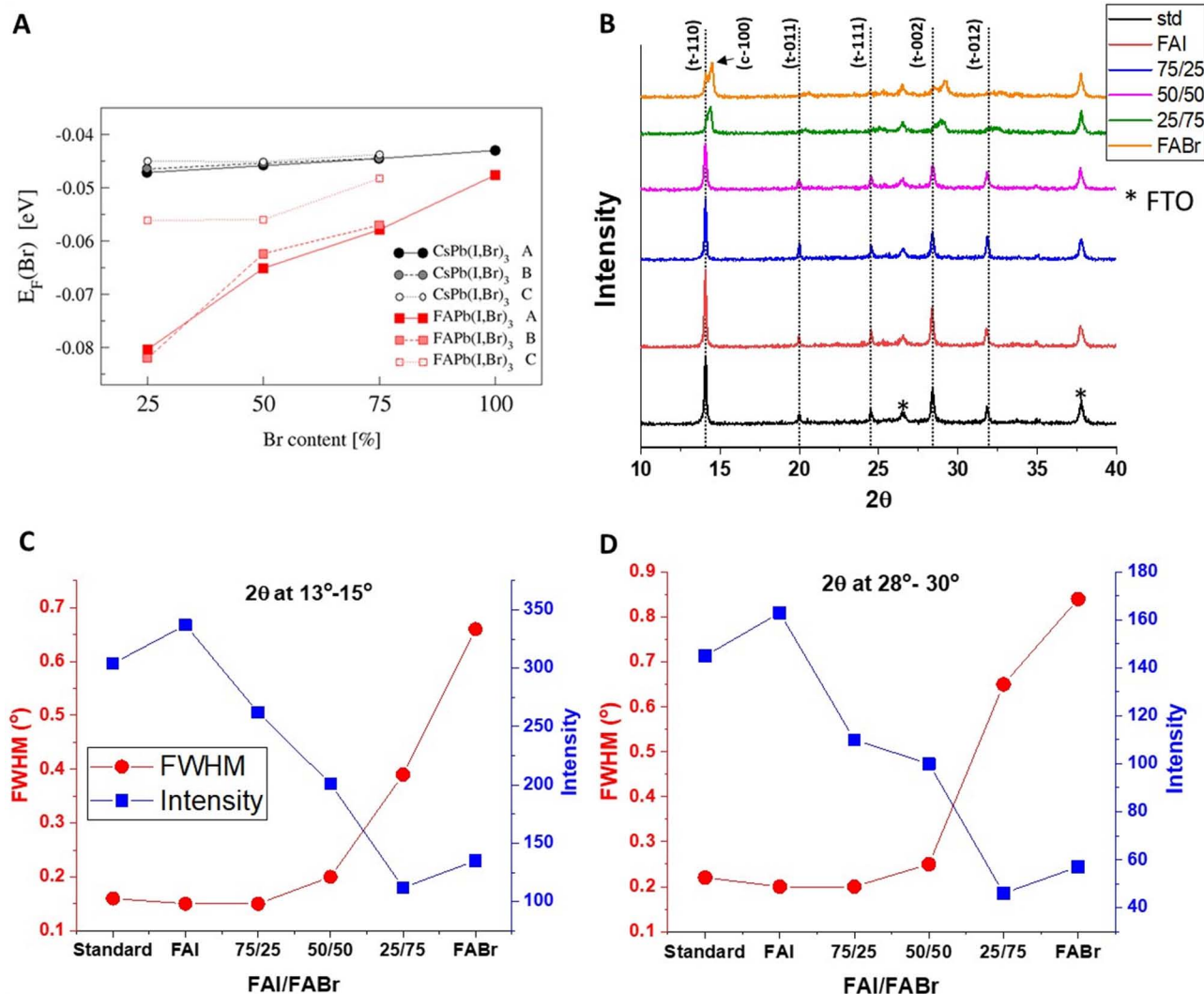
Figure 2. A) Formation energy as function of Br content for CsPb(I,Br)$_3$ and FAPb(I,Br)$_3$ perovskites, where A—avoiding Br–Pb–Br neighborhood, B—between A and C, and C—clustering Br–Pb–Br. B) XRD spectra for mixed cation mixed halide films treated with different ratios of FAI/FABr solutions. The FWHM and the peak intensity located at C) 13–15° and D) 28–30° as a function of the FAI/FABr ratios in the dipping solution.

However, following the post-treatment, when the bromide is incorporated into the perovskite structure, instead of the relatively large iodide (an ionic radius of 1.96 Å for iodide),[34] the already twisted X—Pb—X bond angles are distorted even further, due to volume changes, which results in reducing the crystal symmetry. In the case of high FAI ratios (pure FAI and 75/25 solutions), there is no peak splitting or shifting in the XRD spectra because the majority in the synthesized perovskite film are iodide (the standard perovskite film without the post-treatment). Therefore, the crystallographic planes are adjusted mostly according to the iodide size. Hence, incorporating iodide into the existing lattice results in less (or almost nothing) distortion of the crystal structure.

To additionally verify this chemical replacement, we performed density functional theory (DFT) calculations for the $2 \times 2 \times 2$ supercells of FAPb(I$_{1-x}$Br$_x$)$_3$ and CsPb(I$_{1-x}$Br$_x$)$_3$, for the Br content $x = 25\%$, 50%, 75%, and 100%. We confirm that all formation energies are negative and reported in Figure 2A (given for one I into Br exchange). Since the distribution of 24 iodide ions in a supercell into 6, 12, and 18 Br atoms—for $x = 25\%$, 50%, and 75%, respectively—might be done in many ways, we have chosen three doping patterns: A—"avoiding Br–Pb–Br neighborhood", C—"clustering Br–Pb–Br", and B—"between A and C." The optimized atomic structures for these distributions are shown in Figures 1S and 2S, Supporting Information. The halide-exchange formation energies for the Cs-cation perovskite are a bit smaller than these numbers for the FA-cation perovskite. But the most pronounced difference between these crystals, with respect to I-into-Br replacement, is in the role of Br distribution: cases A, B, and C have very similar formation energies for CsPb(I$_{1-x}$Br$_x$)$_3$, while the clustering of Br–Pb–Br bonds (case C) is visibly less favorite scenario than the uniform spread of Br in the FAPb(I$_{1-x}$Br$_x$)$_3$ crystal. This is in contrast to the basic semiconductors used for traditional electronic devices—such as Si,

GaN, ZnO—where a clustering of the impurity atoms is difficult to avoid during doping, and especially unwanted in the diluted magnetic semiconductors.

Absorbance measurements were performed on the post-treated perovskite films to determine whether there was any effect on the film's absorbance due to dipping in the FAI/FABr solution. As can be seen in **Figure 3**A, there is a blue shift in the absorbance when the FABr ratio increases and a red shift when the FAI ratio increases. This indicates that a halide exchange occurs in the already crystalized perovskite film. To confirm that there is no cation exchange at the A site between Cs^+ and FA^+, we measured the absorbance spectra of $Cs_{0.2}FA_{0.8}PbI_3$ films with and without dipping in the pure FAI solution, as shown in Figure S3, Supporting Information. No spectral shift in the absorbance onset was observed for the dipped and for the nondipped films. It is expected that with cation exchange some structural changes in the lattice would occur, resulting in a shift in the absorbance and the XRD spectra.[13,32]

Interestingly, in the case of dipping in pure FABr (orange curve), a second absorbance and photoluminescence (PL) peaks can be observed around the 650 and 710 nm wavelength respectively, which can indicate phase segregation in the case of a high FABr ratio and a partial destruction of the perovskite structure.

PL measurements are shown in Figure 3B. A blue shift can be seen when the film was dipped in a pure FABr solution, whereas there was a significant red shift in the PL when the film was dipped in the pure FAI solution. The mixed FAI/FABr solution displays a relatively red or blue shift in the peak maxima that corresponds to the FAI/FABr ratio. These results are consistent with the absorbance measurements. As can be seen in Figure 3C, when FABr is added to the dipping solution, a widening of the PL peak can be observed, in particular, a large increase in the FWHM is observed when there is more than 50% FABr (i.e., pure FABr and 25/75), which indicates an increased number of defects in the perovskite. In addition, an overlap of two PL peaks is observed for pure FABr and 25/75, which indicates the formation of a secondary phase and a nonuniform halide distribution in the perovskite lattice. These features of PL, especially the peak broadening in the Br-rich samples, are consistent with the negative formation energies for all types of the Br distributions and the fact that each Br pattern is associated with a different energy gap.[35]
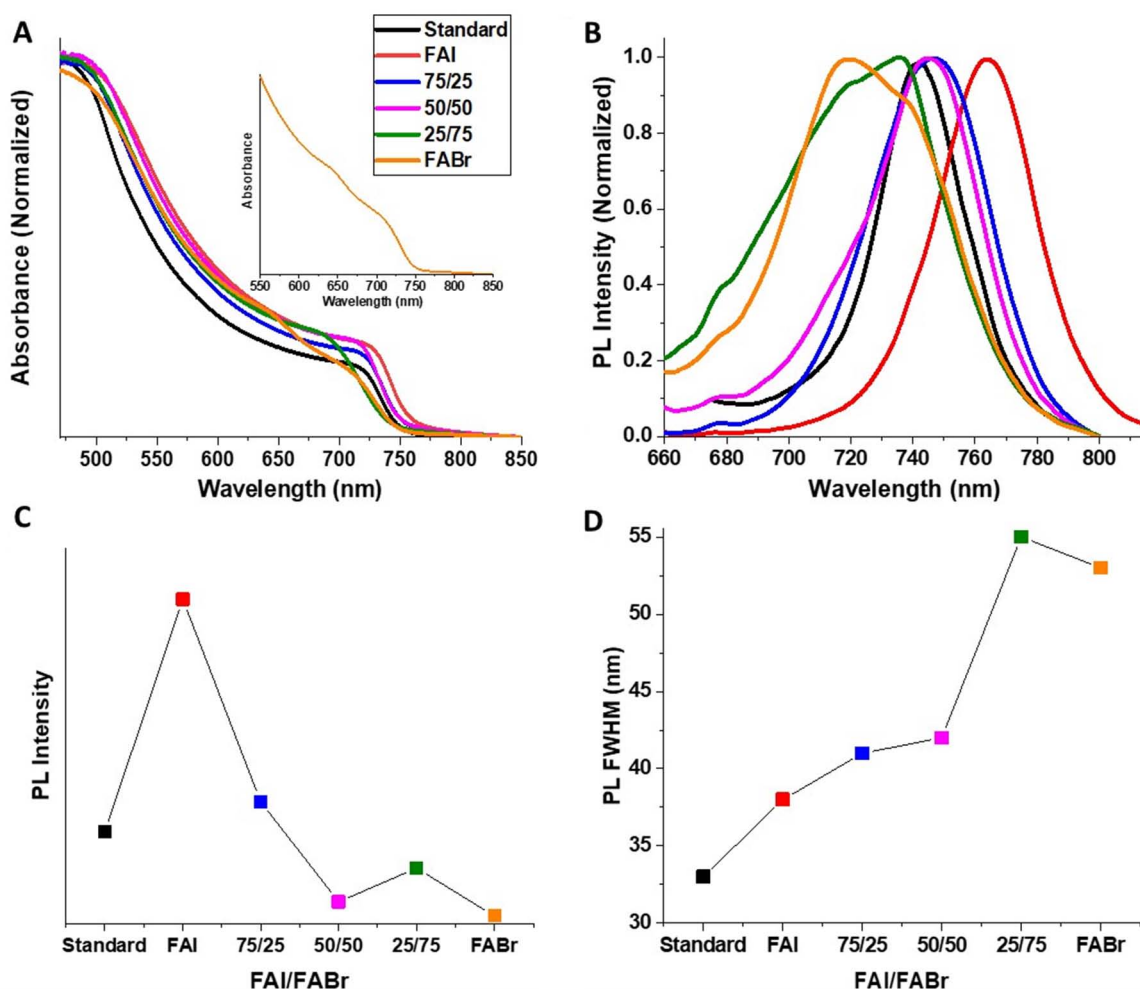

Figure 3. Optical characterization of films treated with different FAI/FABr ratios. A) Absorbance and B) PL measurements. C) The FWHM and D) peak intensity values of the PL as a function of the FAI/FABr ratios.

During the halide exchange process, it is possible that some of the halides are not incorporated into the PbX_6 octahedra; instead, some voids are created, which leads to deep-level defects that form mid gap states in the bandgap. These mid gap states are alternative sites for electrons and holes that reduce the potential of the cell,[36] as will be discussed later. These deep-level defects contribute to Shockley–Read–Hall (SRH) recombination, which can be reflected in the peak intensity of the PL in these samples (Figure 3D). The PL measurements were performed on mesoporous TiO_2. An increase in the PL intensity can be seen for both the pure FAI and 75/25 post-treated films, whereas in the case of an excess of FABr in the dipping solution (including the 50/50 sample), the PL intensity was low compared with the standard film. The decreased PL intensity in the case of an excess of FABr is mainly due to an increase in the nonradiative SRH recombination and the density of traps, which results from the structural distortion in the perovskite lattice.[37,38]

The morphology of three post-treated films (pure FAI, FAI/FABr 50/50, and pure FABr) and pure IPA dip were characterized by scanning electron microscopy (SEM) before and after the treatment, as shown in **Figure 4**. No significant change can be recognized in the grain size of the perovskite films as a result of the post-treatment. Although the post-treatment does not affect the grain size, it can be seen that as the FABr ratio increases, the morphology is affected and the shape of the crystals become more cubic and pin holes start to appear in the film. This observation supports the claim that some crystal distortion exists at a high FABr ratio and the fact that bromide is introducing into the crystal lattice, as it is also indicated by the XRD measurements.

The examination of theoretically obtained crystal structures, for various Br-doping concentrations and distributions, sheds more light into the grain size and pin holes. Let us compare again Figures 1S and 2S, Supporting Information. When Br atoms concentrate around the same Pb atom, then the chemical bonds between Br and Pb surrounded by iodides tend to break due to the longer interatomic distances. This scenario is realized in the distributions of C-type and would lead to the formation of cracks between the grains. On the other hand, experimentally, the grain size almost does not change with the excess of FABr. This is because, as mentioned earlier, the formation energy for case C is less favorite than it is for the more uniformly distributed replacements with Br (cases A and B). These energetically favorable distributions are characterized with the point-like broken bonds Br—Pb, which do not form the crack lines but the small pin holes. Interestingly, the organic cations (FA) seem to adjust their orientations to the pattern of the Br distribution, i.e., the clustered cases (C-type) possess very well-ordered molecular phase. This fact, in turn, might affect the speed of molecular rotations[39] and the bandgaps breathing.[35]

X-ray photoelectron spectroscopy (XPS) measurements were performed to get an indication of the halide exchange as a result of the post-treatment in the already crystalized perovskite films.

The atomic concentrations of bromide and iodide in the perovskite films for treated and nontreated films can be observed in Table S1, Supporting Information. With high FAI ratios (FAI and 75/25), the amount of bromide decreases due to the iodide incorporation, whereas for high FABr ratios, the bromide atomic concentration increases and the iodide atomic concentration decreases. In films that were treated with the same ratio of FAI and FABr (50/50), the bromide atomic concentration was slightly higher than the iodide atomic concentration compared with the standard film. This observation can be explained by bromide having smaller radii than iodide does, which permits faster diffusion in the solution than the iodide does and a better overlap with the Pb^{2+} orbitals,[18] giving some preference to bromide incorporation over iodide. Moreover, the large lattice expansion and the lack of a thermodynamic driving force slows down the replacement of bromide by iodide.[30] The trend of the halide exchange as a function of the FAI/FABr ratio can also be seen in Figures S5A and S5B, Supporting Information, which present the XPS peaks for bromide and iodide, respectively.

An important observation was derived from the energy-dispersive spectroscopy (EDS) line scan measurement on a cross-section made by focused ion beam (FIB). This measurement proves that bromide incorporates into deep regions of the perovskite film and does not present only on the surface. The EDS line scan
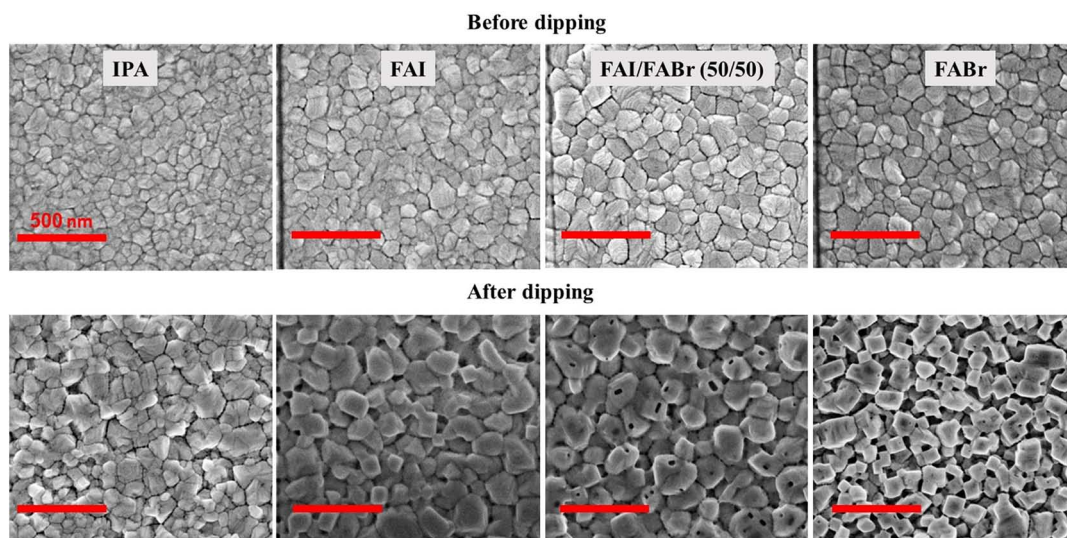

Figure 4. SEM images of $Cs_{0.2}FA_{0.8}Pb(I_{0.75}Br_{0.25})_3$ perovskite films before and after post-deposition treatment with IPA, FAI, FAI/FABr - 50/50, and FABr.

was measured on $Cs_{0.2}FA_{0.8}PbI_3$ film and on the same film after the FABr post-treatment (**Figure 5**A,B, respectively). It can be seen that in the case of nontreated film there is no indication of bromide, whereas in the case of FABr post-treated film, the presence of bromide can be found along the whole film, in addition to the iodide. Still, the amounts of iodide and bromide are different as supported by the optical measurements; however, the presence of bromide inside the film proves that the reaction is not only on the surface.

In the next stage, the influence of the post-treatments on the perovskite film in a complete solar cell was studied. The solar cell's structure, which was used in this work, was composed of mesoporous TiO_2, which functions as the electron transporting layer (ETL), and Spiro-OMETAD, which functions as the HTM. Apparently, the changes in the perovskite lattice, as a result of the halide exchange, influence the extracted charges in the solar cell. **Figure 6**A shows charge extraction measurements that were performed on a complete solar cell with and without the post-treatment. The charge extraction measurements consist of several steps: at the beginning (the cell is not connected) the cell is illuminated for 2 s (called the illumination time); following the illumination, the light is switched off for a certain time (delay time);

then, the cell is connected and the charges that were left are extracted from the cell. This measurement is repeated for several delay times. It can be observed that the standard cell has more charges to extract for the whole range of delay times, compared with the post-treated solar cells, which have fewer charges to extract for the same range of delay time.

The high FABr ratio (25/75) and pure FABr in the dipping solution shows that already after a short delay time there are fewer charges to extract, compared with the case of a low FABr ratio (75/25) and an equal FAI/FABr (50/50) ratio, where there are more charges to extract for the same delay time. In addition, the voltage decay measurements that follow the voltage drop as a function of time show the same trend as the charge extraction (Figure 6B). With high FABr ratios, the voltage decay is much faster than with a high FAI ratio in the dipping solution. The drop in voltage is even slower with the nontreated cell (i.e., the standard). Based on a previous study,[40] the remaining voltage (around 300 mV) with the nontreated cell can be related to the charge accumulation, which can be assigned to the inner electric field across the junction and to an additional electrostatic potential that contributes to the standard build in potential, therefore, increasing the overall voltage of the cell, in agreement with the
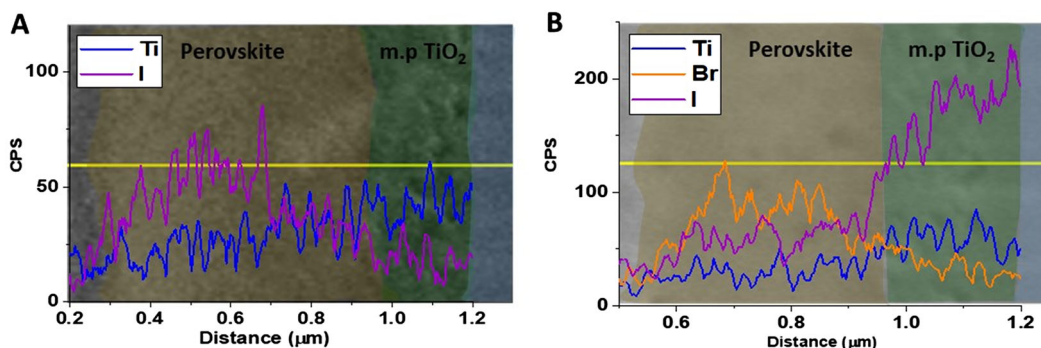

Figure 5. EDS line scan on cross-section of perovskite film made by FIB. A) $Cs_{0.2}FA_{0.8}PbI_3$ perovskite film (nontreated film). B) FABr post-treated $Cs_{0.2}FA_{0.8}PbI_3$ film.
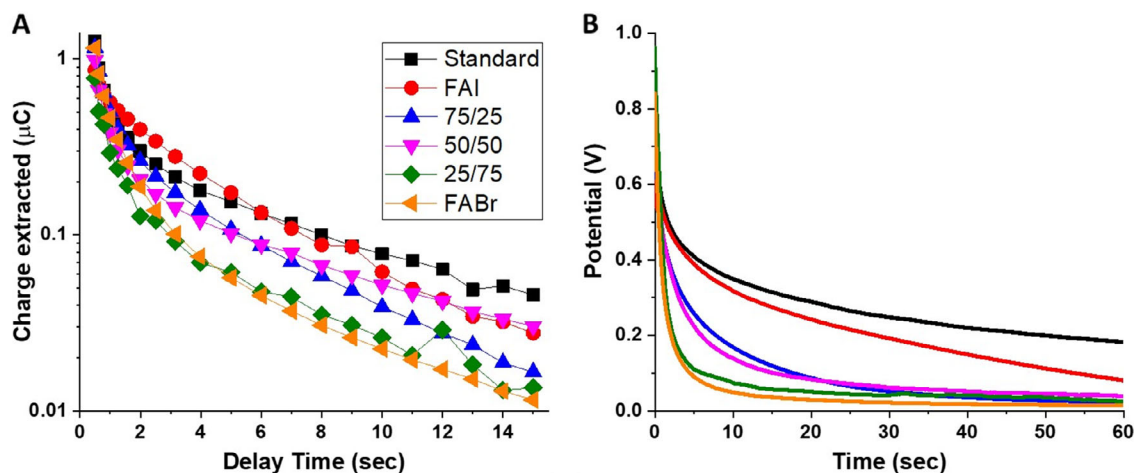

Figure 6. A) Charge extraction measurements and B) Voltage decay measurements for solar cells fabricated with post-treatments (FAI/FABr ratios) and without post-treatment.

Table 1. Average PV parameters of the different FAI/FABr ratios. The best PV parameters are shown in brackets.

V_{oc} [V]	J_{sc} [mA cm^{-2}]	Fill factor [%]	Efficiency [%]	Dipping conditions [FAI/FABr]
1.06 ± 0.02 (1.04)	19 ± 1 (21.1)	65 ± 6 (74.9)	13 ± 2 (16.6)	None
0.98 ± 0.04 (0.99)	20 ± 3 (22.4)	67 ± 3 (72.0)	13 ± 2 (15.9)	FAI
0.98 ± 0.08 (1.10)	21 ± 1 (20.2)	65 ± 4 (71.7)	13 ± 1 (16.0)	75/25
0.99 ± 0.06 (1.11)	20 ± 1 (19.7)	64 ± 7 (71.3)	13 ± 2 (15.6)	50/50
0.99 ± 0.04 (1.01)	18 ± 2 (19.6)	62 ± 5 (69.7)	11 ± 2 (13.8)	25/75
0.98 ± 0.03 (1.04)	18 ± 1 (18.7)	58 ± 7 (69.2)	10 ± 2 (13.5)	FABr

PV results below, as shown in **Table 1**. To conclude, these observations are in good agreement with the physical and optical characterizations that show distortion of the perovskite lattice in the case of high FABr ratios in the dipping solution, which are also expressed in the complete solar cells.

Table 1 presents the average (15 cells for each condition) PV performance of the post-treated and nontreated cells. The average PV parameters are similar for the standard and for cases with an excess of FAI including a 50/50 ratio. However, when there is an excess of FABr in the dipping solution, the average PV parameters decrease to 11% and 10% PCE, on average. The best PV parameters for each condition are shown in brackets in the table, and their corresponding *JV* curves are shown in Figure S6A, Supporting Information. The current densities of the cells as a function of time are shown in Figure S6B, Supporting Information, which show that a steady state for each condition was reached. Interestingly, in all cases, except for an excess of FABr in the dipping solution, the current increases in the first 5 s before reaching a steady state. However, in the case of

excess FABr, the current density decreases slowly. During the halide exchange, there are ion vacancies that redistribute under external bias and enhance the electric fields, which result in decreased J_{sc}.[41] The average V_{oc} value of the post-treated cells is lower than that of the standard cells. This is due to the halide exchange process in the perovskite film that probably cause some halide voids, which lead to mid-gap states, as discussed earlier.

Stability measurements were performed under continuous 1 sun illumination in ambient air for over 40 min using four cycles of illumination (12 min) and 4 min in the dark. The measurements were made on post-treated and standard cells by tracking their PV parameters (**Figure 7**). The efficiency (Figure 7A), V_{oc} (Figure 7E), J_{sc} (Figure 7D), and the fill factor (FF) (Figure 7B) decrease with time for all cell types. The FF and the efficiency of the cells, which were post-treated with relatively low FABr ratios, recover after 4 min in the dark; on the other hand, with the high FABr ratios, the recovery after each cycle is much smaller. The V_{oc} value of the nontreated cell (standard) almost completely recovers to its initial value after each 4 min in the dark, whereas
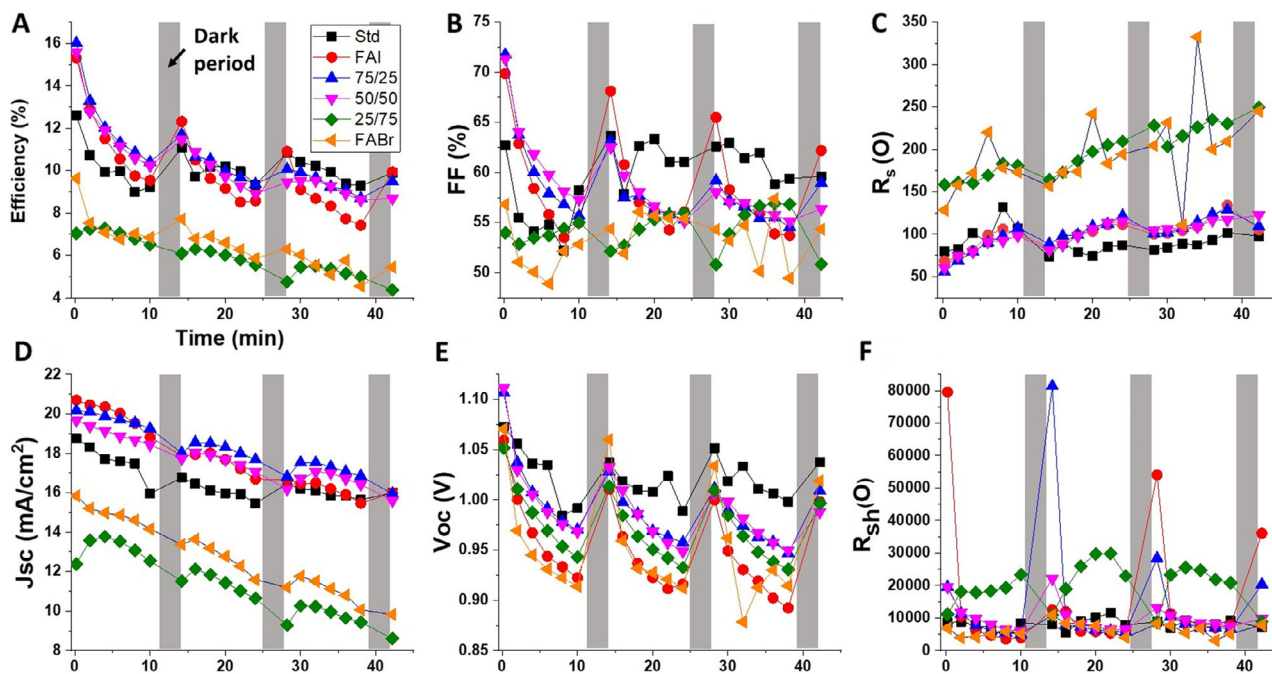

Figure 7. Stability measurements under 1 sun illumination in ambient air. Three cycles in the light were performed with 4 min in the dark (gray area) between each cycle. The PV parameters are shown in A) efficiency, B) FF, C) series resistance, D) current density, E) open-circuit voltage, and F) shunt resistance.

the post-treated cells recover but decrease slowly after each cycle. The J_{sc} value decreases constantly for all cell types; note that the high FABr ratio-treated cells display the largest current loss after three illumination cycles. We also tracked the changes in the series and shunt resistances, as shown in Figures 7C,F, respectively. The behavior of the resistances can explain the changes in the FF, since they are related to each other. It can be seen that over time the series resistance increases, whereas the shunt resistance decreases, which results in a reduction of the FF. With pure FAI and 75/25 (FAI/FABr), there is a significant recovery after time in the dark, which results in an improvement of the FF. Moreover, the series resistance of pure FABr and 25/75 (FAI/FABr) post-treated cells display a continuous increase with illumination time along with a slight recovery after 4 min in the dark. This further supports the notion that the charge extraction at the perovskite/selective contacts' interface is problematic, which might be due to the structural changes in the case of bromide exchange.

3. Conclusions

Here, we demonstrated the halide exchange process in the already crystalized perovskite film. Mixed cation mixed halide perovskite film of the structure $Cs_{0.2}FA_{0.8}Pb(I_{0.75}Br_{0.25})_3$ was deposited and post-treated with FAI/FABr ratios in the dipping solution. The post-treated perovskite films displayed a clear shift in their emission and absorbance spectra compared with the standard nontreated films, as a result of the halide incorporated into the perovskite lattice. We found that in the case of an excess of FABr in the dipping solution, there is more distortion in the perovskite structure. The incorporation of small halide instead of iodide affects the crystal structure, which is reflected in the XRD spectra, XPS, PL, and absorbance. EDS line scan measurement on a cross-section made by FIB show that the bromide is present inside the film following the post-treatment, which support the fact that the reaction is not occurring solely on the surface. With complete solar cells, charge extraction and voltage decay measurements displayed enhanced recombination in the post-treated films, especially in those with an excess of FABr. We propose that in the case of significant halide exchange in the perovskite structure, mid gap states are formed as a result of ion vacancies and broken chemical bonds Pb—Br, due to the longer interatomic distances in comparison with pure bromide perovskite. Therefore, the main recombination process in these films is related to SRH recombination, as supported by the peak intensities of the PL. The PV parameters did not display any change in the case of excess FAI in the dipping solution, compared with the standard cells, whereas in the case of excess FABr, the PV parameters were lower, in agreement with the optical, physical, and complete cell characterizations as well as the calculated negative formation energies for the I into Br atom replacement, accompanied by the structural destruction.

Supporting Information

Supporting Information is available from the Wiley Online Library or from the author.

Conflict of Interest

The authors declare no conflict of interest.

[1] S. D. Stranks, G. E. Eperon, G. Grancini, C. Menelaou, M. J. P. Alcocer, T. Leijtens, L. M. Herz, A. Petrozza, H. J. Snaith, *Science* **2013**, *342*, 341.

[2] C. Wehrenfennig, M. Liu, H. J. Snaith, M. B. Johnston, L. M. Herz, *J. Phys. Chem. Lett.* **2014**, *5*, 1300.

[3] D. Shi, V. Adinolfi, R. Comin, M. Yuan, E. Alarousu, A. Buin, Y. Chen, S. Hoogland, A. Rothenberger, K. Katsiev, *Science* **2015**, *347*, 519.

[4] Y. Zhao, A. M. Nardes, K. Zhu, *J. Phys. Chem. Lett.* **2014**, *5*, 490.

[5] G. E. Eperon, S. D. Stranks, C. Menelaou, M. B. Johnston, L. M. Herz, H. J. Snaith, *Energy Environ. Sci.* **2014**, *7*, 982.

[6] M. R. Filip, G. E. Eperon, H. J. Snaith, F. Giustino, *Nat. Commun.* **2014**, *5*, 5757.

[7] A. Amat, E. Mosconi, E. Ronca, C. Quarti, P. Umari, M. K. Nazeeruddin, M. Grätzel, F. De Angelis, *Nano Lett.* **2014**, *14*, 3608.

[8] J. Burschka, N. Pellet, S. J. Moon, R. Humphry-Baker, P. Gao, M. K. Nazeeruddin, M. Grätzel, *Nature* **2013**, *499*, 316.

[9] Y. Li, K. Lu, X. Ling, J. Yuan, G. Shi, G. Ding, J. Sun, S. Shi, X. Gong, W. Ma, *J. Mater. Chem. A* **2016**, *4*, 10130.

[10] D. Liu, T. L. Kelly, *Nat. Photonics* **2014**, *8*, 133.

[11] M. J. Carnie, C. Charbonneau, M. L. Davies, J. Troughton, T. M. Watson, K. Wojciechowski, H. Snaith, D. A. Worsley, *Chem. Commun.* **2013**, *49*, 7893.

[12] NREL, Best Research-Cell Efficiency Chart, https://www.nrel.gov/pv/cell-efficiency.html, accessed: May 14.

[13] M. Saliba, T. Matsui, J. Y. Seo, K. Domanski, J. P. Correa-Baena, M. K. Nazeeruddin, S. M. Zakeeruddin, W. Tress, A. Abate, A. Hagfeldt, *Energy Environ. Sci.* **2016**, *9*, 1989.

[14] N. J. Jeon, J. H. Noh, W. S. Yang, Y. C. Kim, S. Ryu, J. Seo, S. Il Seok, *Nature* **2015**, *517*, 476.

[15] H.-S. Kim, C. Lee, J.-H. Im, K.-B. Lee, T. Moehl, A. Marchioro, S.-J. Moon, R. Humphry-baker, J.-H. Yum, J. E. Moser, *Sci. Rep.* **2012**, *2*, 1.

[16] F. Hao, C. C. Stoumpos, D. H. Cao, R. P. H. Chang, M. G. Kanatzidis, *Nat. Photonics* **2014**, *8*, 489.

[17] J. H. Noh, S. H. Im, J. H. Heo, T. N. Mandal, S. Il Seok, *Nano Lett.* **2013**, *13*, 1764.

[18] C. Yi, J. Luo, S. Meloni, A. Boziki, N. Ashari-Astani, C. Grätzel, S. M. Zakeeruddin, U. Röthlisberger, M. Grätzel, *Energy Environ. Sci.* **2016**, *9*, 656.

[19] M. Saliba, J. P. Correa-Baena, C. M. Wolff, M. Stolterfoht, N. Phung, S. Albrecht, D. Neher, A. Abate, *Chem. Mater.* **2018**, *30*, 4193.

[20] J. W. Lee, D. H. Kim, H. S. Kim, S. W. Seo, S. M. Cho, N. G. Park, *Adv. Energy Mater.* **2015**, *5*, 1501310.

[21] W. Tan, A. R. Bowring, A. C. Meng, M. D. McGehee, P. C. McIntyre, *ACS Appl. Mater. Interfaces* **2018**, *10*, 5485.

[22] T. Singh, T. Miyasaka, *Adv. Energy Mater.* **2018**, *8*, 1700677.

[23] M. A. Green, A. Ho-Baillie, H. J. Snaith, *Nat. Photonics* **2014**, *8*, 506.

[24] Z. Li, M. Yang, J. S. Park, S. H. Wei, J. J. Berry, K. Zhu, *Chem. Mater.* **2016**, *28*, 284.

[25] D. B. Mitzi, *Progress in Inorganic Chemistry*, Vol. *48*, Wiley-Blackwell, New York **2007**, pp. 1–121.

[26] K. T. Cho, S. Paek, G. Grancini, C. Roldán-Carmona, P. Gao, Y. Lee, M. K. Nazeeruddin, *Energy Environ. Sci.* **2017**, *10*, 621.

[27] H.-S. Yoo, N.-G. Park, *Sol. Energy Mater. Sol. Cells* **2018**, *179*, 57.

[28] M. Wang, *ACS Appl. Mater. Interfaces* **2018**, *10*, 37005.

[29] M. Rai, S. Rahmany, S. S. Lim, S. Magdassi, L. H. Wong, L. Etgar, *J. Mater. Chem. A* **2018**, *6*, 23787

[30] N. Pellet, J. Teuscher, J. Maier, M. Grätzel, *Chem. Mater.* **2015**, *27*, 2181.

[31] Y. H. Chang, C. H. Park, K. Matsuishi, *J. Korean Phys. Soc.* **2004**, *44*, 889.

[32] L. K. Ono, E. J. Juarez-Perez, Y. Qi, *ACS Appl. Mater. Interfaces* **2017**, *9*, 30197.

[33] M. I. Saidaminov, A. L. Abdelhady, G. Maculan, O. M. Bakr, *Chem. Commun.* **2015**, *51*, 17658.

[34] L. Atourki, E. Vega, B. Marí, M. Mollar, H. Ait Ahsaine, K. Bouabid, A. Ihlal, *Appl. Surf. Sci.* **2016**, *371*, 112.

[35] M. Wierzbowska, J. J. Meléndez, D. Varsano, *Comput. Mater. Sci.* **2018**, *142*, 361.

[36] W. J. Yin, T. Shi, Y. Yan, *Adv. Mater.* **2014**, *26*, 4653.

[37] J. W. Lee, S. H. Bae, N. De Marco, Y. T. Hsieh, Z. Dai, Y. Yang, *Mater. Today Energy* **2018**, *7*, 149.

[38] T. Du, J. Kim, J. Ngiam, S. Xu, P. R. F. Barnes, J. R. Durrant, M. A. McLachlan, *Adv. Funct. Mater.* **2018**, *28*, 1801808.

[39] C. Quarti, E. Mosconi, J. M. Ball, V. D'Innocenzo, C. Tao, S. Pathak, H. J. Snaith, A. Petrozza, F. De Angelis, *Energy Environ. Sci.* **2016**, *9*, 155.

[40] R. Gottesman, P. Lopez-Varo, L. Gouda, J. A. Jimenez-Tejada, J. Hu, S. Tirosh, A. Zaban, J. Bisquert, *Chem* **2016**, *1*, 776.

[41] E. L. Unger, E. T. Hoke, C. D. Bailie, W. H. Nguyen, A. R. Bowring, T. Heumüller, M. G. Christoforo, M. D. McGehee, *Energy Environ. Sci.* **2014**, *7*, 3690.